DIGITAL LIBRARY

dspace.vutbr.cz

On the performance of electronically tunable fractional-order oscillator using grounded resonator concept

ŠOTNER, R.; JEŘÁBEK, J.; POLÁK, L.; LANGHAMMER, L.; STOLAŘOVÁ, H.; PETRŽELA, J.; ANDRIUKAITIS, D.; VALINEVICIUS, A.

AEU - International Journal of Electronics and Communications
2021, vol. 129, February 2021, pp. 1-17

ISSN: 1434-8411

DOI: https://doi.org/10.1016/j.aeue.2020.153540

Accepted manuscript

© 2021. This manuscript version is made available under the CC-BY-NC-ND 4.0 license
http://creativecommons.org/licenses/by-nc-nd/4.0/

On the Performance of Electronically Tunable Fractional-Order Oscillator Using Grounded Resonator Concept

Roman Sotner[1*], Jan Jerabek[2], Ladislav Polak[1], Lukas Langhammer[1], Hana Stolarova[1], Jiri Petrzela[1], Darius Andriukaitis[3], Algimantas Valinevicius[3]

[1] Department of Radio Electronics, SIX Research Center, Brno University of Technology, Technicka 3082/12, Brno 61600, Czech Republic
[2] Department of Telecommunications, SIX Research Center, Brno University of Technology, Technicka 3082/12, Brno 61600, Czech Republic
[3] Department of Electronics Engineering, Faculty of Electrical and Electronics Engineering, Kaunas University of Technology, Studentu St. 50-438, LT-51368 Kaunas, Lithuania
[*]corresponding author email: sotner@feec.vutbr.cz

Abstract:

Recent works target the design of fractional-order oscillators. However, some features of such circuits are not frequently considered in the design despite their importance in practice. This work provides an analysis of the fractional-order oscillator design procedure with a simple but still beneficial electronic tuning feature. The presented design allows us to keep a stable and non-standard phase shift between produced harmonic signals while tuning the oscillation frequency of the oscillator. Grounded fractional-order elements and modern commercially available active elements are implemented in the designed topology. Time domain results as well as spectral analysis are obtained from experimental measurements. Moreover, several values of non-standard phase shifts are tested. The experimental verification targets the low-frequency bandwidth from several hundreds Hz up to several kHz because of possible application areas in these bands (audio) and due to a very low-impedance character of the used RC constant phase elements as approximants of fractional-order capacitors.

Keywords:

Constant-phase element, electronic adjusting, fractional-order, oscillator, phase shift, tuning.

1. Introduction

The importance of the fractional-order design [1] is rapidly increasing in various fields. Fractional-order passive elements fit various applications in the circuit design. The design of oscillators with a various and non-standard phase shift between generated harmonic signals represents one of the most important examples of an application of the fractional-order passive elements (the so-called fractional-order capacitors). Table I compares key features of already known solutions presented in literature.

Radwan et al. [2] present results (Fig. 2 in [2]) obtained by the state-variable synthesis in circuits using a single operational amplifier (OA). These topologies are similar to the well-known Wien bridge circuits. The used structures are simple but many passive elements (including fractional-order devices) are floating. In [3], several solutions employing operational transresistance amplifiers (OTRAs) as active elements (AEs) are introduced. Once again, many passive elements need to be used in a floating position. In [4], a more sophisticated synthesis based on multi-loop feedback systems has been selected in case of multiphase solutions utilizing current conveyors (CCs) and OAs. Current feedback operational amplifiers (CFOAs) and CCs are employed similarly in [5]. However, in all multiphase cases, the operation is supposed only for the fixed frequency of oscillation (FO). Said et al. [6] introduced very simple structures using a single OA and an impedance converter (gyrator).

The detailed study of the impact of a particular value of order on the oscillation frequency and the obtained value of the phase shift are given. Kartci et al. [7] proposed an interesting structure employing several CMOS transistors forming basic building elements as operational transconductance amplifiers (OTAs) and voltage buffers (VBs). Their work [7] presents the results of tests of behavior for several different cases of order selection. A significant simplification of this concept was shown in [8], where two OTAs and two VBs were used. The tested topology includes only three passive elements. Two CFOAs and six passive elements (fractional-order devices in grounded form) are used in the solution that was introduced in [9]. However, operational voltages (amplitudes) of these circuits are quite nonrealistic because of their values (above the supply level in some cases). An oscillator, based on the Colpitts topology, using a floating fractional-order was analyzed in [10]. Three fractional-order passive elements are included in this design that is more typical for multiphase oscillators than for two-phase ones. In [11], the commonly known topology of the Wien bridge oscillator was tested with fractional-order elements replacing standard capacitors. A very similar single-active-device based LC topology with solid-state representation of the fractional-order device (similarly to [11]) was presented in [12]. This work clearly shows how the implementation of fractional-order elements, compared to solutions using standard integer-order capacitors, helps with shifting the oscillation frequency to higher values. However, the electronic tuning of FO is not a subject of study in these works. Work [13] showed a simple topology using differential difference current conveyors (DDCCs) and grounded passive elements. This is a significant advantage in comparison with many recent works. Further simplification was reached in case of the solution presented in [14].

There is only one AE (voltage differential inverted and buffered amplifier, abbreviated as VDBI) having features similar to [11] and [12]. In [15], three DDCCs as AEs including all grounded passive elements were also selected for a multiphase design. It indicates that a complex active device (internal principle) can significantly help with the implementation of grounded passive elements. On the other hand, individual transistors as the simplest active devices can be also used in the design of fractional-order oscillators [16]. In [15], the active device, used in topology allowing grounded CPEs, is similarly complex as device in our work. Additional value of our proposal, in comparison to [15] (see **Table 1** for further details), is that it provides benefits regarding easy electronic tunability, phase shift maintained constant, etc. in comparison to the topologically simplest solutions (for example [16]). Electronically tunable features of a multiphase sinusoidal fractional-order oscillator were studied and practically tested in [17] for the first time. However, as will be discussed later, some important features of this oscillator are not discussed. Various approximation techniques for the design of a fractional-order approximant by passive RC sections were explored in several types of oscillators using the Wien bridge family and a single OA [18]. The fractional-order oscillators using OAs were also studied in two OAs-based structures [19]. Despite of a detailed analysis of theoretical FOs and conditions of oscillation (COs) [18], [19] showing interesting features, their concepts are similar to previous works using Wien-based topologies and have typical disadvantages (e.g. too many and floating passive elements and missing electronic tunability). On the other hand, the low-impedance voltage outputs represent an important benefit of OA-based solutions. The general multiphase solution of the oscillator in [20] shows how the order and the number of low-pass sections (three were used in the discussed example) impact the value of the oscillation frequency and the start-up condition. However, practical information about electronic tunability and stability of output levels is not discussed. Moreover, work [20] is not solving unequal values of orders of the used fractional-order capacitors. An interesting attempt leading to the voltage control of FO was shown in [21]. Unfortunately, an operable implementation is obtained only for equal orders of both fractional-order capacitors and the phase shift between the output levels is not constant. The same team of authors extended their useful work by a detailed analysis of various structures [22]. They reported the widest frequency tunability range (up to hundreds of kHz) from available works and results. There are variants of fractional-order oscillators using three (voltage multiplier-based) advanced AEs that predetermine simple electronic tunability (unfortunately in specific cases only [22] and the phase shift is dependent on the driving voltage).

Table 1. Comparison of important features of the known solutions of fractional-order oscillators.

Ref. (Fig. in reference)	Number of active elements	Number of passive elements	Number of fractional-order elements (all grounded – Yes/No)	Unequal orders of fractional-order elements	Simple design equations with low number of terms	FO independent on CO	Single-parameter electronic tunability of FO available	Tested electronic tunability in simulation/experiment (frequency range)	Phase shift maintained constant during the tuning process	Amplitude ratio maintained constant during the tuning	Amplitude stabilization implemented
[2] (Fig. 2)*	1	5-6	2 (No)	Yes	Yes	Yes	N/A	N/A (single tone)	Yes	N/A	No
[2] (Fig. 7a)	1	7	3 (No)	Yes	a	Yes	N/A	N/A (single tone)	N/A	N/A	No
[2] (Fig. 7b)	1	4	3 (No)	Yes	No	Yes	N/A	N/A (single tone)	N/A	N/A	No
[3]	1-2	4-7	2 (No)	Yes	a	Fig. 2e,f,h	N/A	N/A	a Fig. 2e,f,h	N/A	No
[4]	3-4	8	4 (Yes)	Yes	No	N/A	N/A	N/A	N/A	N/A	No
[5]	7-8	7-8	3 (Yes)	Yes	No	a	N/A	N/A	N/A	N/A	No
[6] (Fig. 11,12)	1-2	7	2 (No)	Yes	No	Yes	N/A	N/A (single tone)	a	N/A	No
[7]	4	2	2 (No)	Yes	No	N/A	N/A	N/A	N/A	N/A	No
[8]	1	3	2 (No)	Yes	No	N/A	N/A	N/A	No	No	No
[9]	2	6	2 (Yes)	Yes	No	Yes	N/A	N/A	N/A	N/A	No
[10]	5	4	3 (No)	Yes	No	Yes	N/A	N/A	N/A	N/A	No
[11]	1	6	2 (No)	No	N/A	N/A	N/A	N/A	N/A	N/A	No
[12]	1	5	1 (Yes)	No	No	Yes	N/A	N/A	N/A	N/A	No
[13]	2	4	2 (Yes)	Yes	Yes	No	N/A	N/A	N/A	N/A	No
[14]	1	4	2 (No)	Yes	No	Yes	N/A	N/A (single tone)	N/A	N/A	No
[15]	3	6	3 (Yes)	Yes	No	No	b	N/A	N/A	N/A	No
[16]	1	4	3 (No)	Yes	No	N/A	N/A	N/A	N/A	N/A	No
[17]	3	5	2 (No)	Yes	Yes	N/A	Yes	2.5→50 kHz	Yes	N/A	No
[18]	1	5-6	2 (No)	Yes	Yes	Yes	N/A	N/A	N/A	N/A	No
[19]	2	6	2 (No)	Yes	No	Yes	N/A	N/A	No	N/A	No
[20]	3	3	3 (Yes)	No	No	Yes	Yes	10.4→5.1 kHz	Yes	No	No
[21]	3	5	2 (Yes)	Yes	a	a	Yes	N/A	No	N/A	No
[22]	3	5	2 (Yes)	Yes	a	Yes	Yes	?→ 450 kHz	No	N/A	No
[23]	2	3	2 (Yes)	No	Yes	Yes	N/A	0.8→5.7 kHz	Yes	a	Yes
Proposed	4	5	2 (Yes)	Yes	Yes	Yes	Yes	2.5→41 kHz 0.4→1.6 kHz 0.1→0.9 kHz 0.4→2.5 kHz 0.3→1.2 kHz 0.3→1 kHz	Yes	a	Yes

*Wien type circuit with amplifier (resistor feedback), the analysis uses the state-variable approach; a - yes in case of equal values of parameters (passive elements) and (or) identical orders of CPEs of presented circuitry; b - tunability possible by time constant (passive element - resistor) and effect of the order on frequency enlargement shown; figures noted in table relate to specific reference! Note that parameters in the table are valid for fractional order behavior and/or $\alpha \neq \beta$ (some referenced papers include also behavior for $\alpha = \beta = 1$ that is not an objective of our interest); ? the low corner of frequency is not written in the paper, the highest frequency reaches from 280 up to 450 kHz; N/A – information not available/shown/analyzed;

Once again, many studied cases indicate the dependence of the value of the phase shift on the driving force (therefore also on FO) and the behavior of output levels when FO tuned is not studied.

Many further important details of the evaluated works are noted in **Table 1**. A deeper analysis of the majority of these works also indicates that the derived design equations are hardly applicable in the straightforward design (hand calculation from directly expressed CO and FO) and, therefore, their immediate usage and calculations are impractical (a polynomial form of the expression for oscillation frequency, numerical software solver required, etc.). Numerous recently presented solutions suffer from

typical drawbacks, for instance: mutual dependence of CO and FO, missing system for amplitude stabilization, and missing or unavailable electronic tuning of FO. In many cases, the change of the phase shift and the amplitude ratio during the tuning process is not studied. These issues make the particular solution less interesting for real application. Unfortunately, almost none of above discussed works is dealing with these important features.

This paper presents a design of a fractional-order oscillator where the above discussed features and issues are addressed. Next, this work offers an overview and a detailed analysis of features that are important for practice and applications. They are simultaneously available in our solution: straightforward design equations, independent FO on the CO, simple electronic tuning (DC voltage control) of FO, phase shift and amplitude ratio constant during the tuning process, and operating amplitude stabilization offering an acceptable distortion of generated waveforms. Moreover, also a study of effects of various orders of CPEs on resulting FO and generated phase shifts of the output waveforms is included.

The rest of this paper is organized as follows: Section 2 introduces the proposed concept of an oscillator using grounded fractional-order elements. Features of the designed constant phase element (CPE) are discussed in Section 3. Results of the experimental analysis of the proposed oscillator are presented in Section 4. Section 5 compares selected experiments with simulation results and evaluates impacts of fabrication dispersions and further mismatches. Section 6 shows a multi-parameter analysis of important design equations in 3D plots and Section 7 evaluates a symbolical sensitivity analysis of the oscillation frequency and conditions on parameters of the circuit. Finally, Section 8 concludes this paper.

2. Proposed structure

The structure of the oscillator is based on the simple principle of the parallel RLC resonator [23]-[26] using a negative resistor (to eliminate damping) and a fractional-order inductor and capacitor (see **Fig. 1**). Nevertheless, solutions presented in [23]-[26] have possible applications in filtering circuits. The idea of the resonator usage in oscillators is not a new phenomenon. However, many standard approaches [27] target only high-frequency and narrow-band tuning features (1.02:1 ratio of min and max FO, see [27]). Therefore, the implementation of resonators in low and medium frequency bandwidths yields a different behavior (necessity of amplitude stabilization for stable and pure sine waves) and wide-band tunability (more than 2:1).

When losses are suppressed by an additional negative resistor ($R_{\mathrm{loss}} = -R_{\mathrm{neg}}$), then the impedance of this resonator in **Fig. 1** has an ideal form (R_{loss} and R_{neg} disappear from the equation when they have equal absolute values [23]-[26]):

$$Z_R(s) = \frac{s^{\alpha} L_{\alpha} R_{loss} R_{neg}}{s^{\alpha+\beta} L_{\alpha} C_{\beta} R_{loss} R_{neg} + s^{\alpha} L_{\alpha} \left(R_{loss} - R_{neg} \right) + R_{loss} R_{neg}} = \left. \frac{s^{\alpha} L_{\alpha}}{s^{\alpha+\beta} L_{\alpha} C_{\beta} + 1} \right|_{\substack{for \\ |R_{loss}| = |R_{neg}|}} . \tag{1}$$

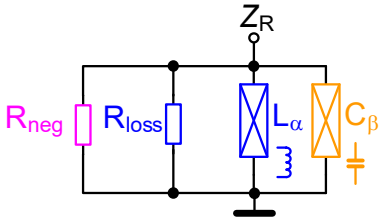

Fig. 1. Principal structure (idea of the concept) of the fractional-order undamped resonator.

For the design of a particular circuit solution using the structure from **Fig. 1**, commercially accessible (off-the-shelf) devices are used because of easy availability of such devices and straightforward verification of the design by laboratory measurements. Its topology, shown in **Fig. 2**, includes two current conveyors of the second-generation (CCII+) [28], [29], one differential difference amplifier (DDA) [28] forming an impedance converter and one variable gain amplifier (VGA) [28] serving to control the negative resistance (voltage adjustability). Two grounded passive CPEs [30], [31], approximating the fractional-order behavior of the fractional-order inductor (L_α after conversion) and the fractional-order capacitor (C_β) in a particular frequency band, are connected to both high-impedance nodes (nodal voltages V_α, V_β). Two optocouplers (OCs), replacing fixed resistors, serve for electronic tunability of the oscillation frequency [32]. The presented topology was derived from our previous proposal [23] and significantly extends the limited initial study with various scenarios and practical experiments. This solution was also added to **Table 1** for comparison of differences between our previous work [23] and the solution presented here (the main difference is in the number of AEs and the lack of electronic DC voltage adjustability – not tested; also identical orders of CPEs were used and therefore many results are not available in [23]). Differences between this work and previous one [23] are shown in detail in **Table 2**.

Table 2. Differences between this work and [23].

	[23]	**This paper**	**Result of the comparison**
Number of passive elements	3 (the CPE is considered as a single element and 2 resistors included inside of hypothetical device)	5 (the CPE is considered as a single element)	Similar
Number of active elements	2 (3 internal sub-blocks; considered as a single hypothetical device with behavioral model)	4	Similar
Tunability	Yes (manual)*	Yes (electronic)	Similar
Single driving force (control voltage) – electronic tunability is tested	No	Yes	Different
Amplitude stabilization is implemented	Yes	Yes	Similar (but specific circuitries and values are different)
Fully operative and complete topology is shown	No	Yes	Different
Tested behavior for different cases of orders and pseudo-capacitance value	No	Yes (several combinations)	Different
Behavior for different cases of orders and pseudo-capacitances supported by 3D plots	No	Yes	Different
Influence of order on phase shift and amplitude levels studied	Yes (for $\alpha = \beta$ only)	Yes (for $\alpha = \beta$, $\alpha \neq \beta$ and combinations of $C_\alpha = C_\beta$, $C_\alpha \neq C_\beta$, where three values of $C_{\alpha,\beta}$ are tested)	Different
Influence of order value on tunability range studied	No	Yes	Different
Tested fabrication dispersion	No	Yes	Different
Tested experimentally (measurements)	No	Yes	Different
Sensitivity analysis	No	Yes	Different
THD analysis	Yes (simulation – single tone)	Yes (experiment and simulation in available bandwidth – dependence)	Different
Errors between theory, simulation and experiment – tested in important cases	No	Yes	Different

*Further implementation of OTA and CCII with controllable g_m and R_X parameters is supposed. In the conference paper [23], the variation of equivalent g_m and R_X values (resistor values) was done manually.

In order to simplify the understanding of the purpose of blocks in **Fig. 2**, the same color scheme as in the case of the ideal concept in **Fig. 1** is used. The optocouplers solve the electronic voltage adjustment of the oscillation frequency. The block for conversion and compensation of driving currents ensures the transformation of the DC voltage V_{SET_FO} to the forward current of both diodes and the symmetric adjustment of $R_{OC1,2}$. Because the diodes in real $OC_{1,2}$ have slightly different threshold voltages and an exponential dependence of the forward current on the forward voltage, some compensation of driving in branches should be taken into account (therefore the R_{pot} used). The blue colored dashed line specifies the part behaving as the resonator itself (including losses). The pink block represents a specific solution of the adjustable negative resistor and the green block shows the connection of the amplitude stabilization discussed in detail in Section 3. The green and brown areas are not a part of the ideal concept in **Fig. 1**.

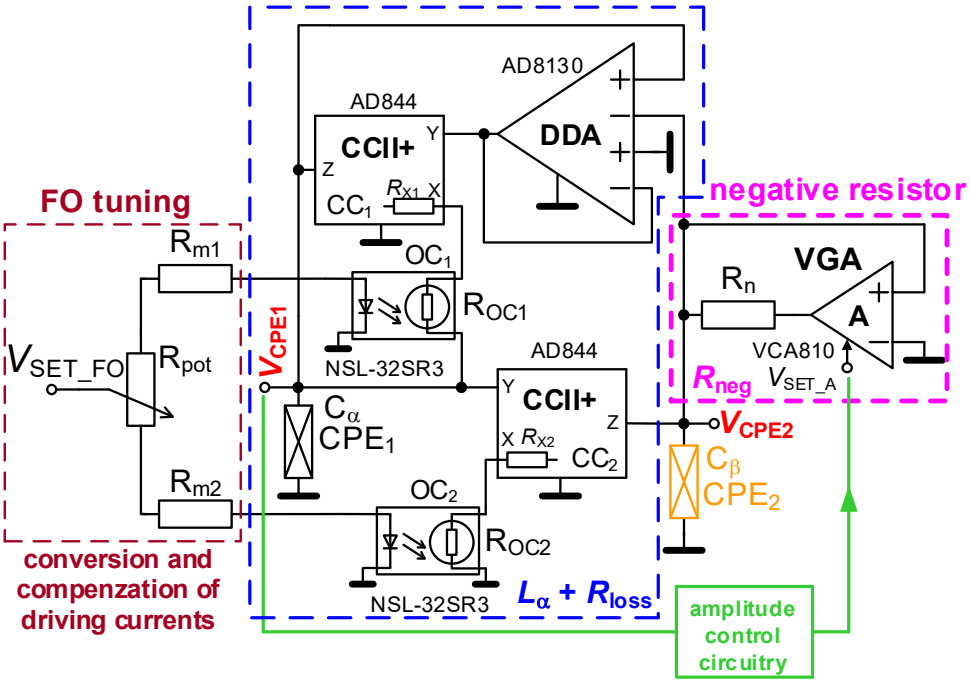

Fig. 2. Designed topology of the practically tested oscillator with off-the-shelf active elements.

We consider V_{CPE2} as an input node. Thereby, the impedance (considered between the node V_{CPE2} and ground) of the resonator (as shown in **Fig. 2**) can be found (now considering all parameters in **Fig. 2** – also expressed R_{neg} by parameters of the full circuitry of the negative resistor: A and R_n) as:

$$Z_R(s) = \frac{s^{\alpha} C_{\alpha} R_{OC1} R_{OC2} R_n}{s^{\alpha+\beta} C_{\alpha} C_{\beta} R_{OC1} R_{OC2} R_n + s^{\alpha} C_{\alpha} R_{OC1} R_{OC2} (1-A) + 2R_n}, \tag{2}$$

where the parameter A represents the gain of the VGA. This parameter is very important for the control of oscillations as shown below. We can see that the term of the denominator starting by s^{α} disappears for $A = 1$. That is the intended effect of the negative resistor in the structure of the resonator (now full oscillator) despite we did not express exactly the value of R_{loss} at the oscillation frequency. The characteristic equation (denominator of (2)) of this circuit has the following form:

$$s^{\alpha+\beta} + s^{\alpha} \frac{(1-A)}{C_{\beta} R_n} + \frac{2}{C_{\alpha} C_{\beta} R_{OC1} R_{OC2}} = 0 \cdot \tag{3}$$

The methodology for analysis of the fractional-order characteristic equation has been presented in [2]-[6] for example. In this work, these methods are used too. The difference is only in obtainment of the

analyzed equations ([2] and many further works used the state-variable approach. Our work uses an impedance expression. This equation can be rearranged by the Euler formula to:

$$\begin{aligned}&\omega_0^{\alpha+\beta}\left[\cos\left((\alpha+\beta)\frac{\pi}{2}\right)+j\sin\left((\alpha+\beta)\frac{\pi}{2}\right)\right]+\\&+\omega_0^{\alpha}\left[\cos\left(\alpha\frac{\pi}{2}\right)+j\sin\left(\alpha\frac{\pi}{2}\right)\right]\cdot\left(\frac{1-A}{C_\beta R_n}\right)+\frac{2}{C_\alpha C_\beta R_{OC1}R_{OC2}}=0\end{aligned}. \tag{4}$$

Real and imaginary parts of (4) are defined as, respectively:

$$\omega_0^{\alpha+\beta}\cos\left((\alpha+\beta)\frac{\pi}{2}\right)+\omega_0^{\alpha}\cos\left(\alpha\frac{\pi}{2}\right)\cdot\left(\frac{1-A}{C_\beta R_n}\right)+\frac{2}{C_\alpha C_\beta R_{OC1}R_{OC2}}=0, \tag{5}$$

$$\omega_0^{\alpha+\beta}\sin\left((\alpha+\beta)\frac{\pi}{2}\right)+\omega_0^{\alpha}\sin\left(\alpha\frac{\pi}{2}\right)\cdot\left(\frac{1-A}{C_\beta R_n}\right)=0. \tag{6}$$

Substitution of $\omega_0{}^{\alpha}$ expressed from (6) into (5) yields the frequency of oscillations in the form:

$$\omega_0=\left[\frac{2}{C_\alpha C_\beta R_{OC1}R_{OC2}}\cdot\left(\frac{\cos\left(\alpha\frac{\pi}{2}\right)}{\sin\left(\alpha\frac{\pi}{2}\right)}\cdot\sin\left((\alpha+\beta)\frac{\pi}{2}\right)-\cos\left((\alpha+\beta)\frac{\pi}{2}\right)\right)^{-1}\right]^{\frac{1}{\alpha+\beta}}. \tag{7}$$

This form is more comfortable for the expression of the frequency than other forms typical for fractional-order oscillators and, therefore, also for simple design without calculation of polynomial roots [2]-[10]. The calculation of oscillation frequency from polynomial roots requires a sophisticated software. Parameters R_{OC1} and R_{OC2} (marked as $R_{OC1,2}$) represent the equivalent resistance of optocouplers used for the electronic tuning (DC driving voltage) of the oscillation frequency as will be discussed later. From the eq. (7) we can see that the oscillation frequency is also dependent on the values of the fractional order (α, β) and the values of C_α and C_β. The condition for oscillations (the limit of stability) is obtained from (6):

$$A=1+\frac{\omega_0^{\alpha+\beta}\sin\left((\alpha+\beta)\frac{\pi}{2}\right)C_\beta R_n}{\omega_0^{\alpha}\sin\left(\alpha\frac{\pi}{2}\right)}. \tag{8}$$

The direct form of the gain A expression in (8) clearly indicates the required energy (gain) given by a specific selected oscillation frequency and orders (and values) of the used CPEs. The key parameter for the condition adjustment has been similarly expressed for example in [13], [15], [19]-[21], [23]. It is clear, that the condition fulfilment depends on the oscillation frequency and orders of CPEs (α, β). Fortunately, the issue of the condition dependency on frequency can be easily solved. When a particular frequency is set, the gain A has to be changed properly. In order to compensate common fluctuations of the required value of A that could disturb fulfillment of (8), a precisely adjusted system of amplitude stabilization (amplitude control system) has to be included. This circuitry is able to compensate gain A variations through the tuning process of the oscillator. The amplitude and phase relation of the generated waveforms is expressed as:

$$\frac{V_{CPE1}}{V_{CPE2}} = \frac{-2}{s^{\alpha} C_{\alpha} R_{OC1}}\bigg|_{s^{\alpha}=(j\omega_0)^{\alpha}} = -\frac{2}{j^{\alpha}} \cdot \left\{ C_{\alpha} R_{OC1} \left[\frac{2\sin\left(\alpha\frac{\pi}{2}\right)}{C_{\alpha} C_{\beta} R_{OC1} R_{OC2} \sin\left(\beta\frac{\pi}{2}\right)} \right]^{\frac{\alpha}{\alpha+\beta}} \right\}^{-1}. \tag{9}$$

Equation (9) is generally valid for both fully independent CPEs and gives a comprehensive view on the amplitude and phase relation of both produced sinusoidal waves [32]. If we suppose $R_{OC1} = R_{OC2} = R_{OC}$, and $C_{\alpha} = C_{\beta} = C$ and equal order of both CPEs ($\alpha = \beta$), the independence of the amplitude ratio on the tuning process is obtained and the phase shift is given by α as follows:

$$\frac{V_{CPE1}}{V_{CPE2}}\bigg|_{\alpha=\beta} = -\frac{\sqrt{2}}{j^{\alpha}} \quad \Rightarrow \quad -\sqrt{2}\exp\left[\alpha\frac{\pi}{2}j\right] = \sqrt{2}\exp\left[\left(\alpha\frac{\pi}{2}+\pi\right)j\right]. \tag{10}$$

This setting is used in some parts of this paper. Otherwise (for $\alpha \neq \beta$), the phase shift is always maintained constant at the value determined by α and the amplitude ratio depends on both the frequency (controlled by $R_{OC1,2}$) and the orders of CPEs (α, β). The equal amplitudes for $\alpha = \beta$ during the tuning process can be obtained when a simple resistor divider is applied at the output having the higher amplitude. The quality of amplitudes in case of $\alpha \neq \beta$ can be obtained only when an automatic gain control circuit is implemented at the wave output where the tuning procedure causes level variation (with clear dependence on oscillation frequency). On the other hand, identical orders are sufficient for practice (design of a specific phase shift between waveforms). The behavior for the case with unequal values of orders is studied to complete the analysis. Detailed numerical multi-parameter (3D) analysis (ideal) is shown in **Section 6** for specific design parameters. However, usefulness of such an approach consists only in possible improvement of the range of tunability in certain cases (orders selection). The recommended procedure of the design starts with the selection of the value of the order (identical for both CPEs) based on the phase determined by (10). Then, the CO is maintained thanks to amplitude stabilization/automatic gain control circuit (AGC) with respect to (8) while changing the FO.

3. Features of particular solutions of constant phase elements

The design of passive RC approximants of the theoretically defined fractional-order capacitor $Z_{CPE}(s) = 1/(s^{\alpha}C_{CPE})$ has been widely studied [1], [30], [31], [33]. There are many useful algorithms for calculation of particular values of individual passive components.

In this paper, we are using approaches proposed by Valsa et al. [30], [31] with a detailed example presented in [33] because of good compromise between the bandwidth, phase ripple and complexity. All CPEs, used in this work, are designed in order to ensure the magnitude of impedances having values less than 10 kΩ in the operational bandwidth. This is important because of real parasitic impedances in the nodes of the circuit (see **Fig. 2**). A significantly low level of the impedance of the working CPEs in proper nodes ensures a minimal impact of real active circuitry on the operation. However, as the consequence, the equivalent capacities are very large (units – hundreds of $\mu F/sec^{1-\alpha}$). The limitation of the Valsa's approximation consists in its invalidity for very low frequencies ($\rightarrow$ 0 Hz) where the impedance does not reach infinity but, due to the presence of the correction element R_p, has a finite value also for 0 Hz. In our design case, this effect starts to be significant for frequencies below 1 Hz (out of the operational range of the system).

The RC approximant of the CPE is shown in **Fig. 3** and the calculated values of the elements are presented in **Table 3**. We selected the values 1/4, 1/2, 3/4 of the CPE and the order α and/or β (when two CPEs C_{α} and C_{β} are used in the application discussed later) with the following designed features: the bandwidth of "constant phase range" at least 100 Hz – 100 kHz (tested experimentally) and the phase

ripple in this band maximally ±4°. The results of laboratory measurements are shown in **Fig. 4**. The example of a Monte Carlo analysis of fabrication dispersion (tolerances of R and C are 1% and 5%) shows the maximal phase variation ±3-4° as shown in **Fig. 5** for α = 0.5, C_α = 56 μF/sec$^{1/2}$.

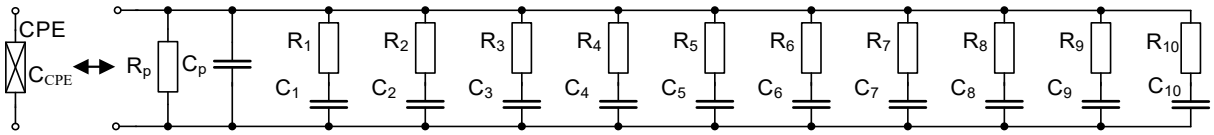

Fig. 3. Passive structure of CPE RC approximant [30], [31] used in oscillator structure as C_α and also C_β.

Table 3. Values of designed CPE RC approximants for three different values of order.

C_{CPE} = 8.8 μF/sec$^{1/4}$ (α = 3/4), C_p = 4.7 pF, R_p = 2.15 kΩ										
i	1	2	3	4	5	6	7	8	9	10
R_k	3.33 kΩ	2.1 kΩ	1.33 kΩ	842 Ω	532 Ω	336 Ω	210 Ω	135 Ω	85 Ω	53 Ω
C_k	3 μF	748 nF	182 nF	49 nF	12 nF	3.3 nF	780 pF	200 pF	50 pF	13 pF
C_{CPE} = 56 μF/sec$^{1/2}$ (α = 1/2), C_p = 0.5 nF, R_p = 15 kΩ										
i	1	2	3	4	5	6	7	8	9	10
R_k	9.1 kΩ	3.65 kΩ	1.46 kΩ	583 Ω	220 Ω	83 Ω	30 Ω	15 Ω	6 Ω	3 Ω
C_k	11 μF	4.4 μF	1.68 μF	680 nF	267 nF	100 nF	38 nF	11 nF	6 nF	3 nF
C_{CPE} = 225 μF/sec$^{3/4}$ (α = 1/4), C_p = 80 nF, R_p = 820 kΩ										
i	1	2	3	4	5	6	7	8	9	10
R_k	1.3 MΩ	268 kΩ	55 kΩ	11 kΩ	2.3 kΩ	463 Ω	100 Ω	20 Ω	4 Ω	0.8 Ω
C_k	7.6 μF	4.4 μF	2.6 μF	1.5 μF	900 nF	538 nF	320 nF	182 nF	101 nF	66 nF

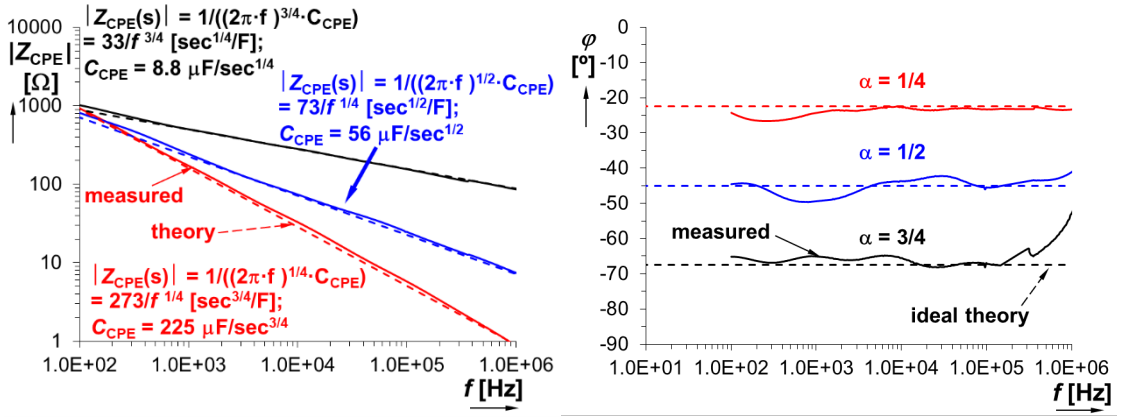

a) b)

Fig. 4. Measured impedance plots of the designed CPE with α = 1/4, 1/2 and 3/4: a) magnitudes, b) phases.

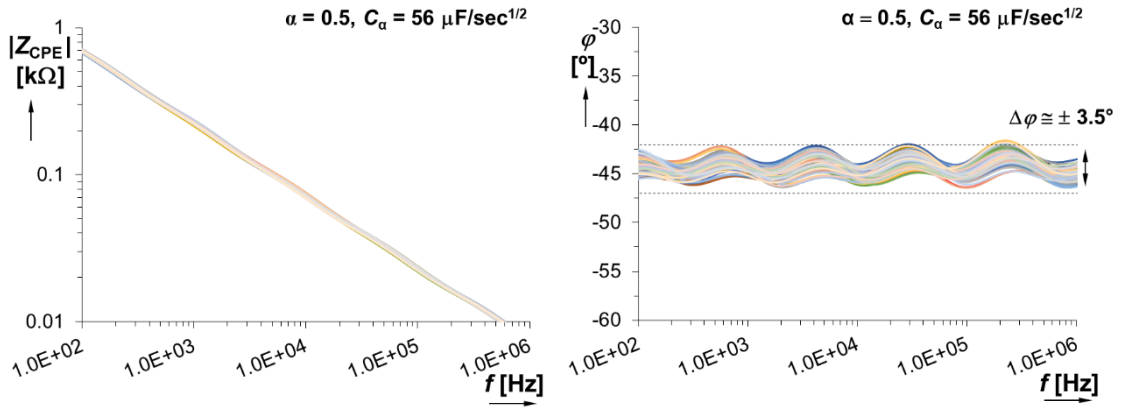

a) b)

Fig. 5. Simulated Monte Carlo variation (fabrication dispersion) of impedance plots of the designed CPE with ($\alpha = 0.5$, $C_\alpha = 56$ µF/sec$^{1/2}$, tolerance R – 1%, C – 5%): a) impedance magnitude plot, b) impedance phase plot.

4. Experimental analysis of the oscillator

The experimental setup, based on **Fig. 2**, uses a circuit for amplitude stabilization [32]. It is shown in **Fig. 6** and its principle is very simple. The waveform from the node V_{CPE1} is amplified by an amplifier using the low-cost opamp (TL072) to the level sufficient for the diode detector using a doubler producing negative DC error voltage. The output levels of the oscillator are expected in hundreds of mV. Therefore, the signal needs to be amplified before processing by a peak detector (doubler). This error voltage is then summed with the "initial" (V_{ini} in **Fig. 6**) constant voltage (slightly higher than required for the startup of oscillations). The resulting DC voltage from the second opamp has a negative polarity because the VCA810 [34] requires negative voltage for its operation. The regulation has a negative feedback character because the increasing input level causes increasing of the negative error voltage and the resulting negative DC voltage for the VCA810 decreases ($V_{ini} - V_{error}$) in the absolute value.

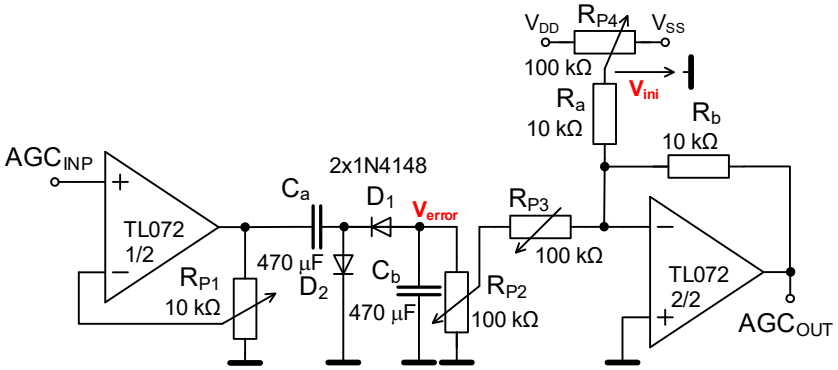

Fig. 6. Circuit for amplitude stabilization and compensation of the oscillation condition (gain A) when oscillator is tuned.

The active circuit elements in the structure of the oscillator, as already indicated in **Fig. 2,** are implemented as follows. The CCII+ is a part of the AD844 [35]. Note that each node of the oscillator was buffered by a voltage buffer available in the package of AD844 [35]. The DDA uses the AD8130 [36] and the negative resistor employs the exponentially driven VCA810 [34], where $A = 10^{2(\mathrm{VSET\_A} - 1)}$. The circuit of the amplitude stabilization and control uses the operational amplifier TL072 [37] (all values are shown in **Fig. 6**). Resistors are implemented by NSL-32SR3 optocouplers [38]. The value of the resistance is numerically equivalent to [32]:

$$R_{OC1,2} \cong 0.2 \cdot \left(\frac{0.5 R_{pot} + R_{m1,2}}{V_{SET\_FO} - V_{th}} \right). \tag{11}$$

We selected the nominal value of $R_{pot} = 2.5$ kΩ (the particular sample had the value of 2.9 kΩ because of common high tolerances of potentiometers), $R_{m1,2} = 910$ Ω and $V_{th} = 1.6$ V [32]. Therefore, the particular value of $R_{OC1,2}$ is dependent on V_{SET_FO} used for the control of FO. The design of the driving circuit (R_{pot} and $R_{m1,2}$) considers currents (hundreds of µA) flowing through the diodes of optocouplers (therefore units of kΩ used) and the available supply voltage (+5 V). The formula for the oscillation frequency (7) can be modified to:

$$\omega_0 \cong \left[\frac{2\left(V_{SET\_FO} - V_{th}\right)^2}{C_\alpha C_\beta \cdot \left[0.2 \cdot \left(0.5R_{pot} + R_{m1,2}\right)\right]^2} \cdot \left(\frac{\cos\left(\alpha\frac{\pi}{2}\right)}{\sin\left(\alpha\frac{\pi}{2}\right)} \cdot \sin\left((\alpha+\beta)\frac{\pi}{2}\right) - \cos\left((\alpha+\beta)\frac{\pi}{2}\right) \right)^{-1} \right]^{\frac{1}{\alpha+\beta}} . \quad (12)$$

Note that the parasitic resistances $R_{X1,2}$ have a significant impact on the results because $R_{OC1,2}$ have very low values expected in hundreds of ohms. Hence, these effects cannot be omitted in the design. The experimental analysis revealed a significant variation of $R_{X1,2}$ (optimistic 50 Ω reported in datasheets [35] can be too far from reality). Therefore, theoretical calculations consider a more realistic value, particularly 100 Ω. However, mismatch of both R_{X1} and R_{X2} values as well as R_{OC1} and R_{OC2} is responsible for further deviations as it is visible in measured results and dependencies. Note that output signals can be directly taken from the voltage buffered (1x) terminals of AD844 [35]. However, the amplitude stabilizing circuit (see **Fig. 6**) has a high-impedance input and can be connected directly to the high-impedance node of the CPE.

4.1 Identical orders

Altogether, three cases are analyzed where the values of orders (α and β) are identical. The resistor of the negative (undamping) impedance was set to R_n = 1 kΩ. Note that to achieve the identical tunability range and the identical change of $R_{OC1,2}$ in all tested cases are not possible due to different features (C_α, C_β) of CPEs. **Figure 7** a) shows the dependence of the oscillation frequency on the V_{SET_FO} driving voltage when both elements have identical values: $C_{\alpha,\beta}$ = 225 μF/sec$^{3/4}$ (α = β = 1/4), $C_{\alpha,\beta}$ = 56 μF/sec$^{1/2}$ (α = β = 1/2) and $C_{\alpha,\beta}$ = 8.8 μF/sec$^{1/4}$ (α = β = 3/4). These selections influence available phase shifts between the generated waveforms as well as the available range of the frequency adjustment and its shift [2]-[11] as derived in the theoretical part. The widest tunability range was obtained for the lowest value of the order. The lowest frequency readjustment is visible for the highest order (→ 1). These expectations are clear from (12). In fact, a specific selection of the order can help with the enlargement of the frequency adjustability range and with these issues in low-voltage designs [11], [15], [17] (limited range of driving voltage). In other words, variation of the order of power in the equation for the oscillation frequency has an effect on the available tunability range when the identical range of driving force is used. However, it is limited by the validity of the approximation of the used CPEs. **Figure 7 b)** depicts the phase shift behavior through the tuning process of the oscillator. As it was expected, certain deviations from the ideal behavior are caused by inaccuracies of CPEs (phase ripples). However, this behavior sufficiently confirms the independence of the phase shift on the tuning process as it was shown in the theoretical equations.

Analysis of three cases of CPEs in the tuning process is summarized in **Table 4**. The CPE $C_{\alpha,\beta}$ = 225 μF/sec$^{3/4}$, having the lowest order α = β = 1/4, leads to the tunability ratio 7:1 (FO_{max}/FO_{min} : $V_{SET\_FOmax}/V_{SET\_FOmin}$), while the values of the phase shift (–157.5° theoretically expected) have the largest deviation from the theory (± 5°). The real transfer features of the active devices and photoresistors and especially coincidences of working fractional-order elements (approximants) and integer-order parasitic capacitances (as parts of terminal impedances) of AEs cause the largest differences between the theory and the experimental results (especially for higher values of FO – case α = β = 1/4). The second case ($C_{\alpha,\beta}$ = 56 μF/sec$^{1/2}$ (α = β = 1/2)) yields significantly narrower tunability ratio (2:1) than the previous case as well as the third case (2.5:1) valid for $C_{\alpha,\beta}$ = 8.8 μF/sec$^{1/4}$ (α = β = 3/4). The example of the output waveform levels and the total harmonic distortion (THD) when the frequency is tuned (for $C_{\alpha,\beta}$ = 56 μF/sec$^{1/2}$ (α = β = 1/2)) is shown in **Fig. 8**. The ratio between the amplitudes corresponds with the equation (10) and it is either √2 or √2/2 (±3 dB). The example of the

output waveforms and a spectral analysis for the particular selected frequency 900 Hz (V_{SET_FO} = 5 V) is depicted in **Fig. 9**. The time domain results in **Fig. 9 a)** show a single tone (fixed frequency) analysis (an example how the results in Fig. 6 and Fig. 7 were obtained). Automatic measurements yield the values of peak-to-peak output levels (133 and 87 mV), the ratio between them (–3.8 dB → 0.65 ≅ √2/2), frequency 1.554 kHz, phase difference between generated waves –131.4° and THD of both waves. The automatic measurement of THD by the DSOX-3022 oscilloscope calculates this value from the peak values of higher harmonic components available in the FFT spectrum (**Fig. 9 b)**). Indicated distances of amplitudes of higher harmonic components to the fundamental tone (dBc) are more than 40 dBc (suppression more than 100 times) that results in values around 1% (very low units of %) [32]. The real results are 1.6 and 1.8% (for both output voltages) as we can see in **Fig. 9 b)**. The results in **Fig. 12** (the same example for different order of both CPEs) are very similar to **Fig. 9** in THD values and phase difference (given by α, therefore the same as in **Fig. 9**). The oscillation frequency is different due to the different dependence of the frequency on the driving voltage (V_{SET_FO} = 5 V) as well as the amplitudes (128 and 66 mV) and their ratio (–5.9 dB → 0.53 ≅ 1/1.9 based on (9)).

Table 4. Numerical results of FO tuning obtained from experiments with CPEs of identical order.

case	C_α [μF/sec$^{1-\alpha}$]	α [-]	C_β [μF/sec$^{1-\beta}$]	β [-]	V_{SET_FO} [V]	Ideal FO range [kHz]	Measured FO range [kHz]	Ideal phase [°]	Measured phase [°]
1	225	1/4	$C_\beta = C_\alpha$	β = α	2.7→5.0	3.17→74	2.50→41	−157.5	−161→−152
2	56	1/2	$C_\beta = C_\alpha$	β = α	2.6→5.0	0.32→1.75	0.40→1.55	−135	−137→−131
3	8.8	3/4	$C_\beta = C_\alpha$	β = α	2.07→5.0	0.12→0.94	0.15→0.90	−112.5	−107→−111

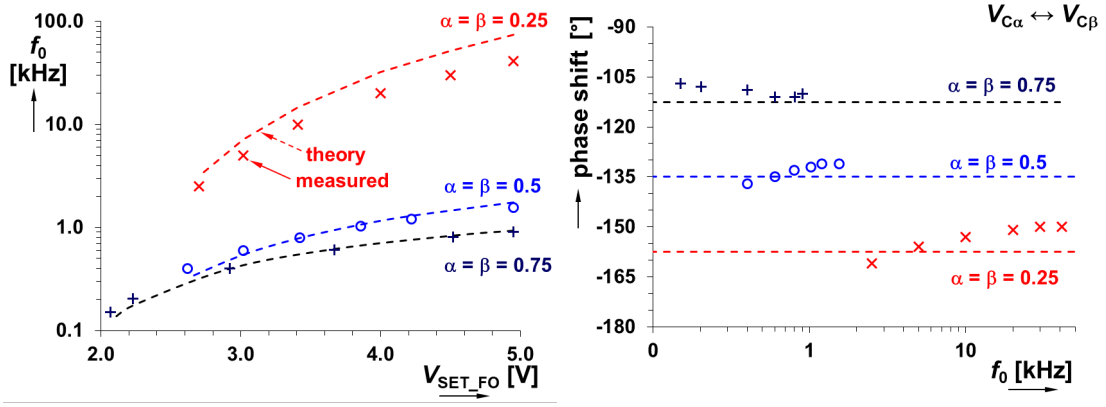

a) b)

Fig. 7. Features of the oscillator when tuning of the oscillation frequency for three values of fractional order (α = β): a) dependence of oscillation frequency on driving voltage, b) dependence of phase shift on oscillation frequency.

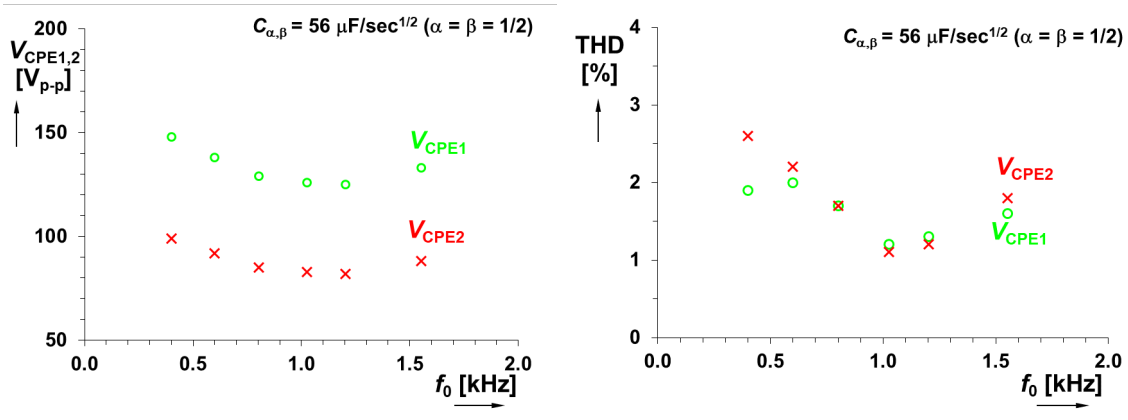

a) b)

Fig. 8. Example of dependences of (valid for $C_{\alpha,\beta} = 56$ μF/sec$^{1/2}$ ($\alpha = \beta = 1/2$)): a) output amplitudes on oscillation frequency, b) THD on oscillation frequency.

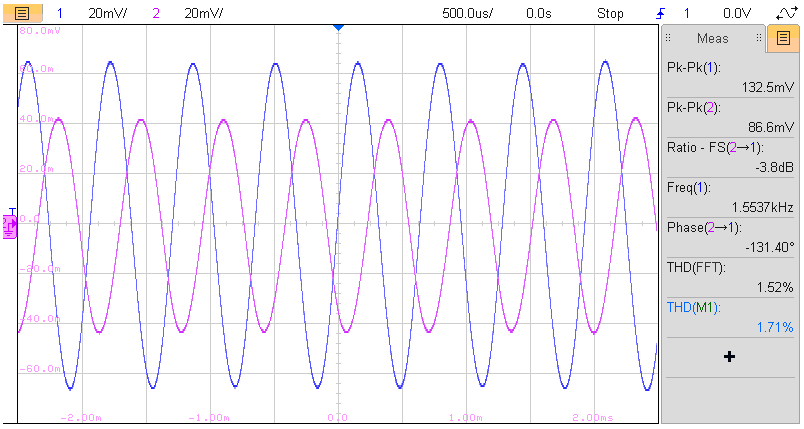

a)

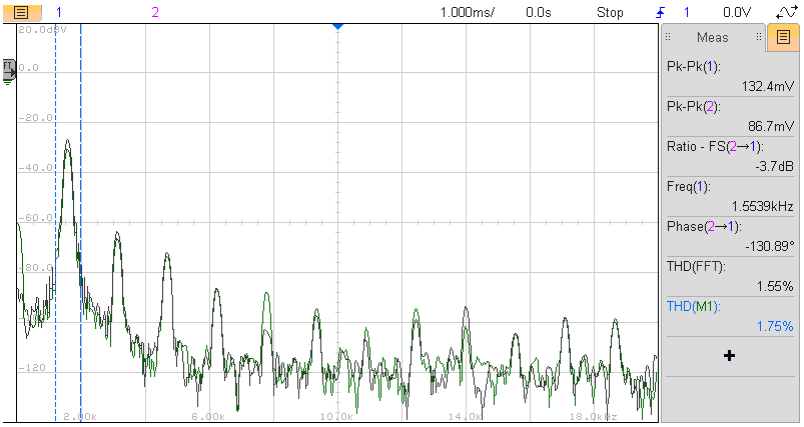

b)

Fig. 9. Example of experimental results (valid for $C_{\alpha,\beta} = 56$ μF/sec$^{1/2}$ ($\alpha = \beta = 1/2$)): a) output waveforms, b) frequency spectrum.

4.2. Example of setting with two different orders

Cases assuming different values of orders ($\alpha \neq \beta$) are also worth investigating as shown in previous works [2]-[10], [13]-[19], [22], [23]. However, the attention is not paid to the impact of the tuning procedure on the phase shift and the amplitude ratio of generated waveforms as shown and analyzed in our contribution. **Figure 10** shows the dependence of the oscillation frequency and the phase shift on the driving voltage. Three cases were studied: $C_\alpha = 225$ μF/sec$^{3/4}$ ($\alpha = 1/4$) together with $C_\beta = 8.8$ μF/sec$^{1/4}$ ($\beta = 3/4$), $C_\alpha = 225$ μF/sec$^{3/4}$ ($\alpha = 1/4$) together with $C_\beta = 56$ μF/sec$^{1/2}$ ($\beta = 1/2$) and $C_\alpha = 56$ μF/sec$^{1/2}$ ($\alpha = 1/2$) together with $C_\beta = 8.8$ μF/sec$^{1/4}$ ($\beta = 3/4$). These sets of values were chosen in order to evaluate the effects of different values of the order of individual CPEs on the FO adjustment as well as the generated phase shift and its variation during the tuning process as derived from expectation [2] in the theoretical part.

An analysis of the tested values of CPEs of different orders in the tuning process is summarized in **Table 5**. The tunability ratio reaches more than 3:1 for the first case and about 2:1 for both remaining cases. In the case of FO tuning, we can see that the largest difference of orders ($\alpha = 1/4$ and $\beta = 3/4$) yields the largest observed range of FO readjustment. This analysis confirms that the phase shift always depends on the order of the capacitor C_α. These interesting features can be utilized in practical designs as follows: the phase shift is determined by a single CPE (C_α) but the range (dependence on driving

force) of the FO readjustment is given by both elements and it can be modified by the second CPE. **Figure 11** analyzes the exemplary results of the amplitude dependence on the oscillation frequency and THD on the frequency for the scenario $C_\alpha = 56$ µF/sec$^{1/2}$ ($\alpha = 1/2$) together with $C_\beta = 8.8$ µF/sec$^{1/4}$ ($\beta = 3/4$). The example of time domain waveforms and the frequency spectrum (selected frequency 1.02 kHz for $V_{SET\_FO} = 5$ V) are captured in **Fig. 12**.The calculation of equation (9) for the used values of CPEs offers the result of the amplitude ratio $V_{CPE1}/V_{CPE2} = 1.9$ (5.6 dB). The experimentally obtained ratio yields 5.9 dB. The results in **Fig. 12** (the same example for different order of both CPEs) are very similar to **Fig. 9** in THD values and the phase difference (given by α, therefore the same as in **Fig. 9**). The oscillation frequency is different due to the different dependence of the frequency on the driving voltage ($V_{SET\_FO} = 5$ V) as well as the amplitudes (128 and 66 mV) and their ratio (–5.9 dB → 0.53 ≅ 1/1.9 based on (9)).

Table 5. Numerical results of FO tuning obtained from experiments with CPEs of different order.

case	C_α [µF/sec$^{1-\alpha}$]	α [-]	C_β [µF/sec$^{1-\beta}$]	β [-]	V_{SET_FO} [V]	Ideal FO range [kHz]	Measured FO range [kHz]	Ideal phase [°]	Measured phase [°]
1	225	1/4	8.8	3/4	2.6→5.0	0.29→2.68	0.40→2.50	–157.5	–160→–155
2	225	1/4	56	1/2	2.7→5.0	0.24→1.15	0.30→1.22	–157.5	–159→–159
3	56	1/2	8.8	3/4	2.5→5.0	0.21→0.97	0.25→1.02	–135	–138→–132

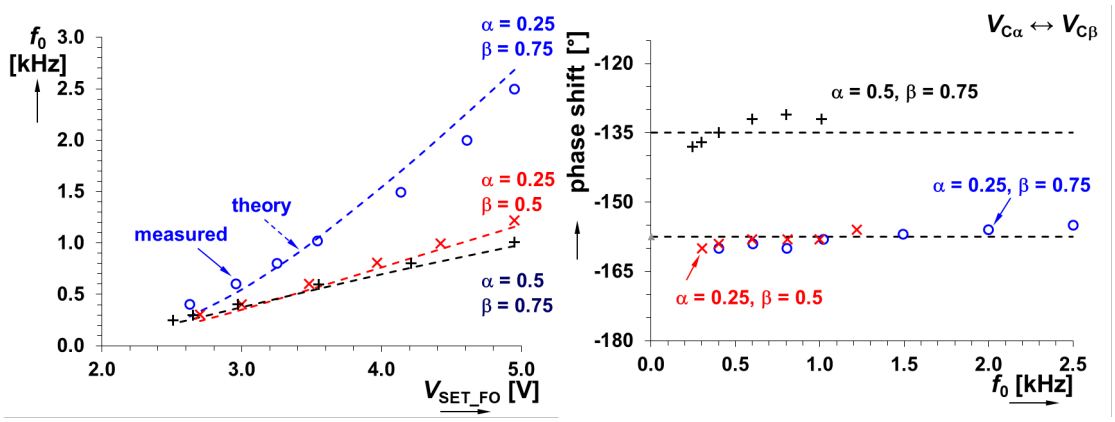

a) b)

Fig. 10. Features of the oscillator when tuning the oscillation frequency for three cases of fractional orders ($\alpha \neq \beta$): a) dependence of oscillation frequency on driving voltage, b) dependence of phase shifts on oscillation frequency.

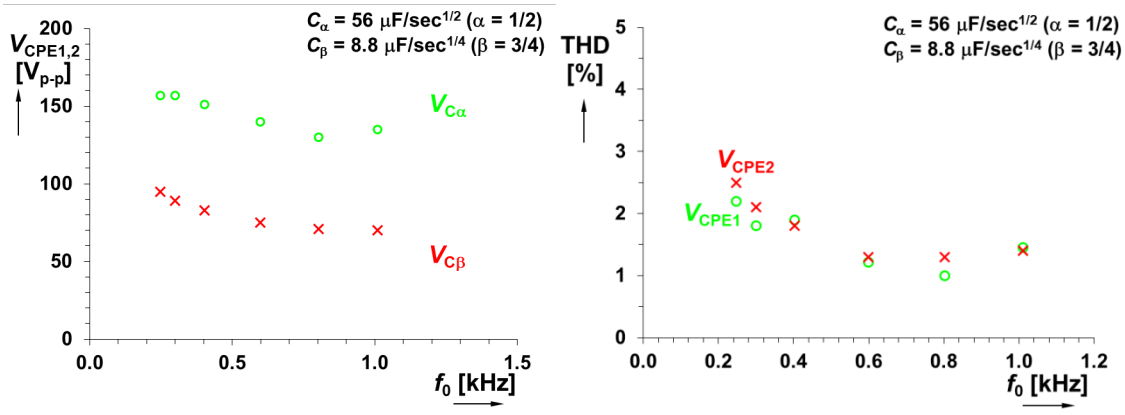

a) b)

Fig. 11. Example of dependences of (valid for $C_\alpha = 56$ µF/sec$^{1/2}$ ($\alpha = 1/2$), $C_\beta = 8.8$ µF/sec$^{1/4}$ ($\beta = 3/4$)): a) output amplitudes on oscillation frequency, b) THD on oscillation frequency.

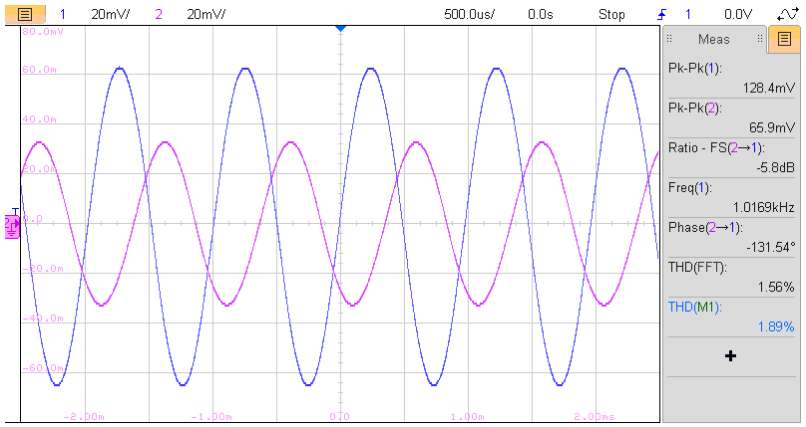

a)

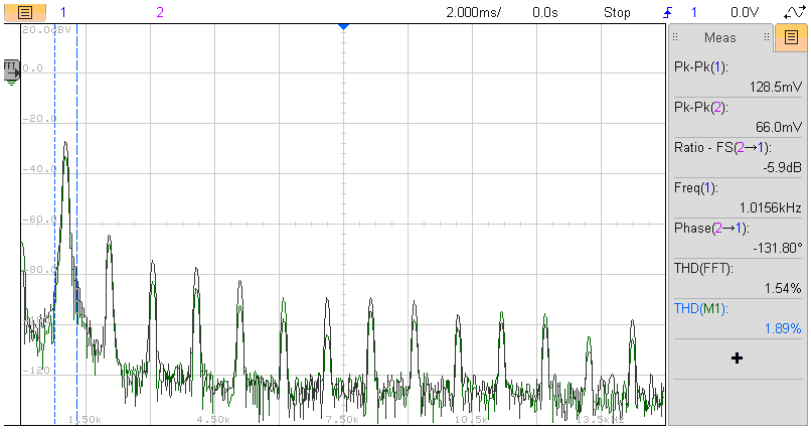

b)

Fig. 12. Example of experimental results (valid for C_α = 56 μF/sec$^{1/2}$ (α = 1/2), C_β = 8.8 μF/sec$^{1/4}$ (β = 3/4)): a) output waveforms, b) frequency spectrum.

5. Comparison of simulation and experimental results of a selected example

The realization of the presented oscillator was tested by the PSpice simulation (all models except an optocoupler are available; the optocoupler was replaced by a standard resistor model and its value in the simulation was adjusted in accordance with the ideal equation (11)). We selected the example of α = β = 0.5. The results are shown in **Fig. 13** where the dependence of the oscillation frequency (as well as related errors between data-points from theory, simulation and experiment) on the driving voltage is given. The maximal deviation of the ideal and the simulated trace in the observed range for the dependence of the frequency on the driving voltage reaches 5%. The error of the measured results vs the ideal trace is below 20% for the lowest frequency and then less than 11% for the rest of the range. These errors are caused by uncertainty and slight variation of the values of fabricated CPEs (C_α, C_β) in the operation frequency range (this value is not fully constant as expected from theory but slightly varies). Further details are available in **Fig. 13**. **Figure 14** indicates that the error of the phase shift between the generated waves does not exceed 6% in all cases. Note that highly similar values and results in amplitudes and THD (high degree of similarity) in simulation and measurement are not possible due to the setting of AGC that is hardly obtainable in identical conditions. In other words, unlike in real experiment (where it is quite easy), it was impossible to set the AGC properly and accurately. Therefore,

error graphs are not plotted for these results. The compared dependences of the output levels and THD on the oscillation frequency are shown in **Fig. 15**. Similar results are expected for other studied cases in this work.

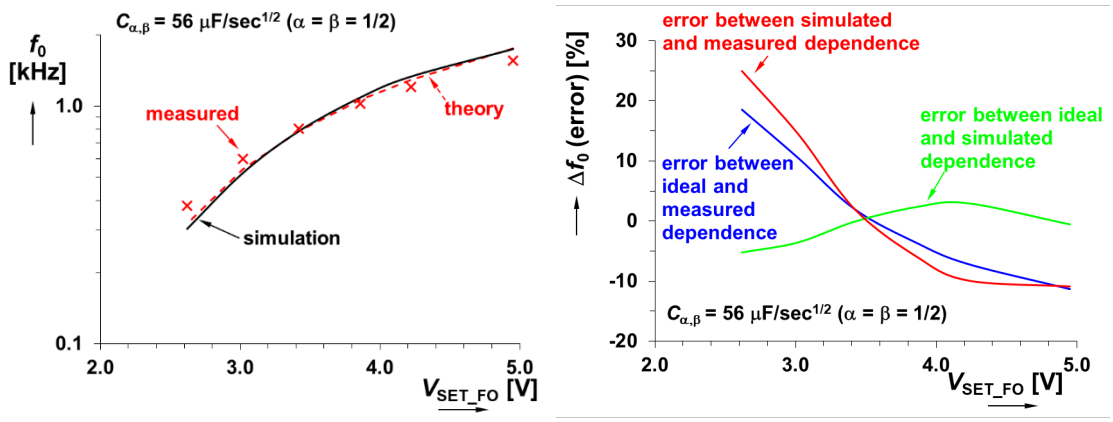

a) b)

Fig. 13. Comparison of experimental, simulated and ideal theoretical dependence of the oscillation frequency on the driving voltage (α = β = 0.5): a) oscillation frequency vs driving voltage, b) error between theory, simulation and experimental results.

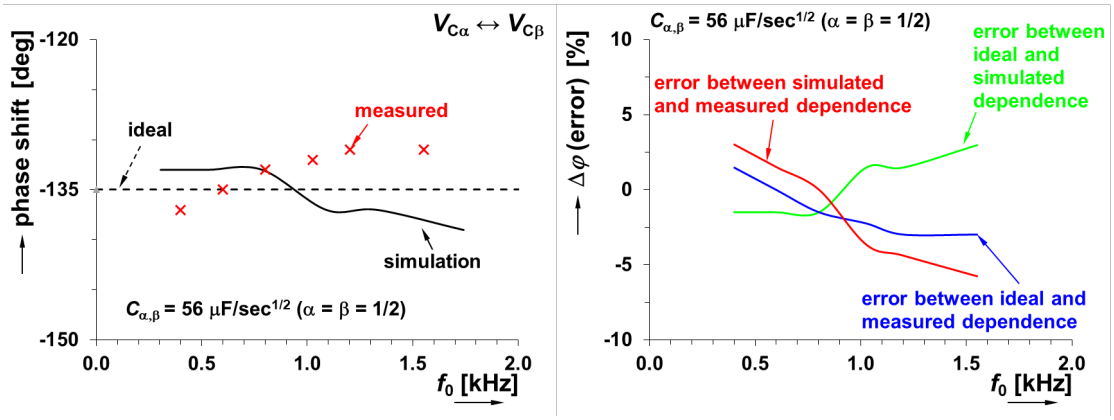

a) b)

Fig. 14. Comparison of experimental, simulated and ideal theoretical dependence of the phase shift on the oscillation frequency (α = β = 0.5): a) phase shift vs oscillation frequency, b) error between theory, simulation and experimental results.

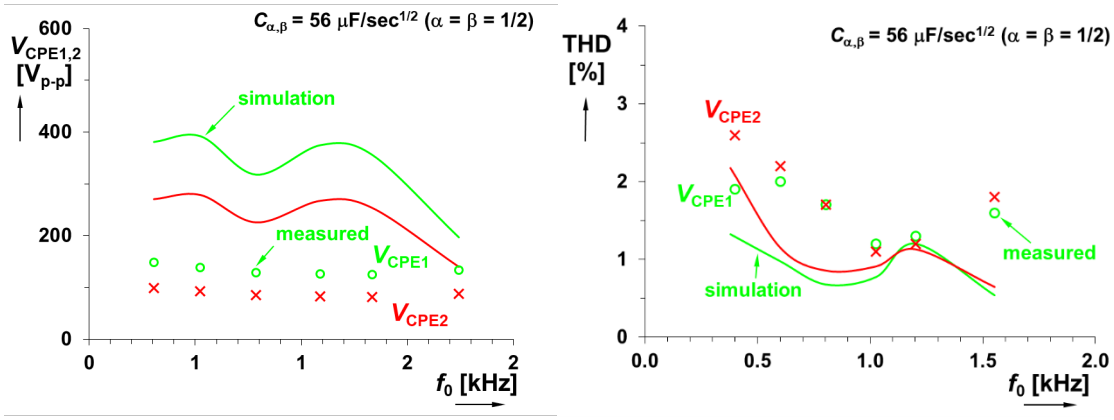

a) b)

Fig. 15. Comparison of experimental and simulated frequency dependence (α = β = 0.5) of: a) output amplitudes, b) THD.

The oscillator shown in **Fig. 2** was tested on the fabrication dispersion of the used CPEs too. A Monte Carlo analysis using tolerances of passive elements applied in structure of CPE (**Fig. 5**) has been provided for full oscillator topology. Only CPEs and passive elements have simulated fabrication dispersion in the following results (for the lowest and the highest oscillation frequencies of the tunability range) because simulation of variations of all values of parameters/components in the complete system was not allowed by the PSpice software (too complex topology, simulation corrupted by limitations of allocated software memory). The allowed number of runs was also limited (100 runs) because of the same reasons. The default design for f_0 = 1.74 kHz (V_{SET_FO} = 5 V) and $C_{\alpha,\beta}$ = 56 μF/sec$^{1/2}$ ($\alpha = \beta = 0.5$) and other parameters noted in this **Section 5** were selected and it represents also the highest value of available f_0 setting. Results are as follows (the maximal limits of variation of the parameters – worst cases ∈ min.↔max.): $V_{CPE1} \in 312 \leftrightarrow 363$ mV, $V_{CPE2} \in 222 \leftrightarrow 251$ mV, amplitude ratio ∈ 1.40↔1.45, oscillation frequency $f_0 \in 1.716 \leftrightarrow 1.851$ kHz, phase shift $\varphi \in 131 \leftrightarrow 149°$. The example of the behavior in frequency spectrum for V_{CPE1} is given in **Fig. 16**. The setting on f_0 = 304 Hz (V_{SET_FO} = 2.6 V) yields Mote Carlo results: $V_{CPE1} \in 309 \leftrightarrow 442$ mV, $V_{CPE2} \in 251 \leftrightarrow 313$ mV, amplitude ratio ∈ 1.39↔1.43, oscillation frequency $f_0 \in 292 \leftrightarrow 313$ kHz, phase shift $\varphi \in 124 \leftrightarrow 146°$. These results indicate that CPEs themselves may have a really significant effect on the obtained deviations in phase (even ±10-11° in the worst case; measurements provided ±3-4°) and frequency (as experimental measurements indicate) even without further influence of AEs.

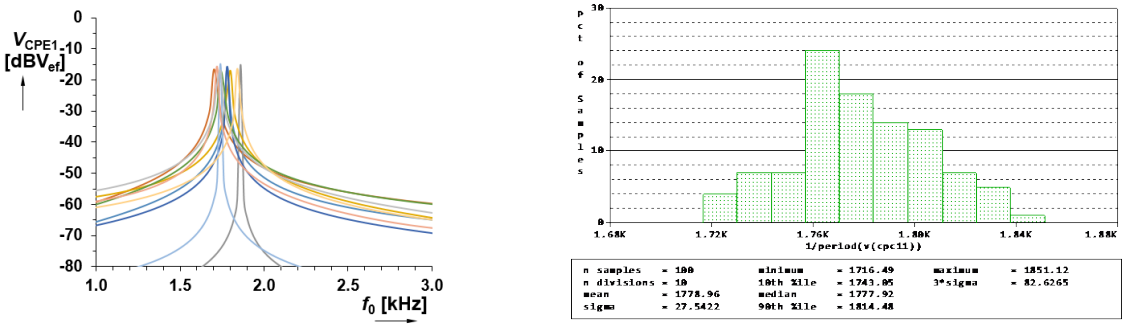

a) b)

Fig. 16. Example of Monte Carlo simulation of fabrication dispersion of passive elements of CPEs (in accordance to behavior in Fig. 5) on oscillation frequency and amplitude of waveform V_{CPE1} shown in: a) detail on 1st harmonic component in FFT spectrum, b) histogram.

Assuming the ideal range of the f_0 adjustment, allowed for the conditions (identical orders 0.5, parameters, etc.) used in **Section 5**, between 321 Hz (for $R_{OC1,2}$ = 563 Ω) and 1750 Hz ($R_{OC1,2}$ = 241 Ω) we expect a substantial impact at higher frequencies. The value of $R_{OC1,2}$ increased by 50 Ω (the expected effect of R_X resistances of AD844 in series with both $R_{OC1,2}$) means more than 500 Hz decrease of f_0 (to 1.2 kHz; decrease more than 30%). This effect is clear because the additional value of R_X means more than 20% deviation. Note that experiments and simulations include the expected effect of R_X. The detailed study of this effect is shown in **Table 6** for additional R_X connected in series to R_{OC1} or R_{OC2} or added to both simultaneously. The described effects can be suppressed significantly when the values of $R_{OC1,2}$ in units of kΩ will be used. However, it depends on the type of the optocoupler - allowed optimal resistivity range. Unfortunately, accuracy of these components is quite limited and unknown in many cases (limited information in datasheets). In addition, the portfolio of these devices is not wide. Further and even more significant mismatch may be caused by the inequality of both $R_{OC1,2}$ due to different dependences of the resistance on the DC current (different diode characteristics of used optocouplers).

Table 6. Effects of influence of serial parasitic resistance $R_{X1,2}$ on oscillation frequency.

parameters	nominal		theoretical expectation		simulation	
	minimum	maximum	minimum	maximum	minimum	maximum
both parameters affected simultaneously						
$R_{OC1,2} + R_{X1,2}$ [Ω]	563	241	563+50 (+9%)	241+50 (+21%)	-	-
f_0 [Hz]	321	1750	270 (–16%)	1200 (–31%)	304 (–5%)	1130 (–35%)
only single parameter influenced						

$R_{OC1} + R_{X1}$ [Ω]	563	241	563+50 (+9%)	241+50 (+21%)	-	-
f_0 [Hz]	321	1750	294 (–8%)	1449 (–17%)	283 (–12%)	1440 (–18%)

6. Multi-parameter analysis of ideal behavior

Theoretical multi-parameter analysis of equations (7) and (9) brings an interesting view on the behavior of the generated frequency and phase shift. The default values and parameters (if not defined as variable later) are the follows: $\alpha = 0.5$, $\beta = 0.5$ (both CPEs have $C_\alpha = C_\beta = 56$ µF and these values are constant during all further tests, only orders vary), $R_{OC1,2} \cong 241$ Ω ($V_{SET\_FO} \cong 5$ V), the theoretical oscillation frequency, phase shift and amplitude ratio for the default parameters reach 1.763 kHz, –135°, and 1.41, respectively. If it is not mentioned, then the invariable parameter (in dependence) is set into the default value above. **Figure 17** shows the dependence of the oscillation frequency on the orders and on the parameter representing the resistance of the optocoupler given in equation (7). The variation of both orders is tested between 0.1 and 1 and the value of $R_{OC1,2}$ (both simultaneously) has the range of adjustability between 200 and 800 Ω. The influence of the order on the frequency has a clear effect and can help with the frequency adjustability range shifting and enlargement, especially in the case of β (see **Fig. 17 b)**). The theoretical tunability range reaches several decades. However, there are significant practical limitations regarding the required phase shift and amplitude ratio as explained later. **Figure 18** analyses the impact of the discussed variations on the amplitude ratio available by equation (9). The results indicate that β has significantly lower impact on the amplitude ratio than α. The results in **Fig. 18** support the expectation that the phase shift is not influenced by β in the case of our circuit. **Figure 19** shows the state of the equality of α and β values. In this case, the amplitude ratio as well as the phase shift are independent on the values of $R_{OC1,2}$ and hence, also on the oscillation frequency.

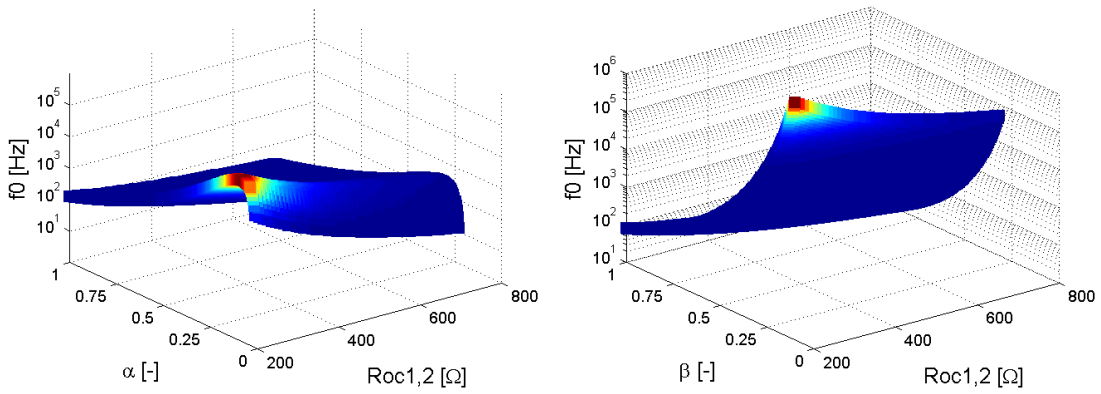

a) b)

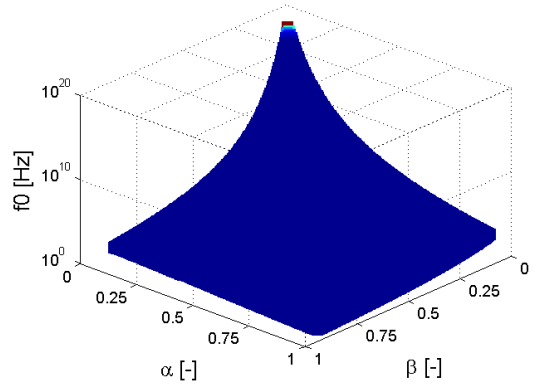

c)

Fig. 17. The 3D analysis of multi-parameter impact (order and parameter for tuning) on oscillation frequency (valid for $C_{\alpha,\beta}$ = 56 µF): a) frequency vs α and $R_{OC1,2}$, b) frequency vs β and $R_{OC1,2}$, c) frequency vs α and β.

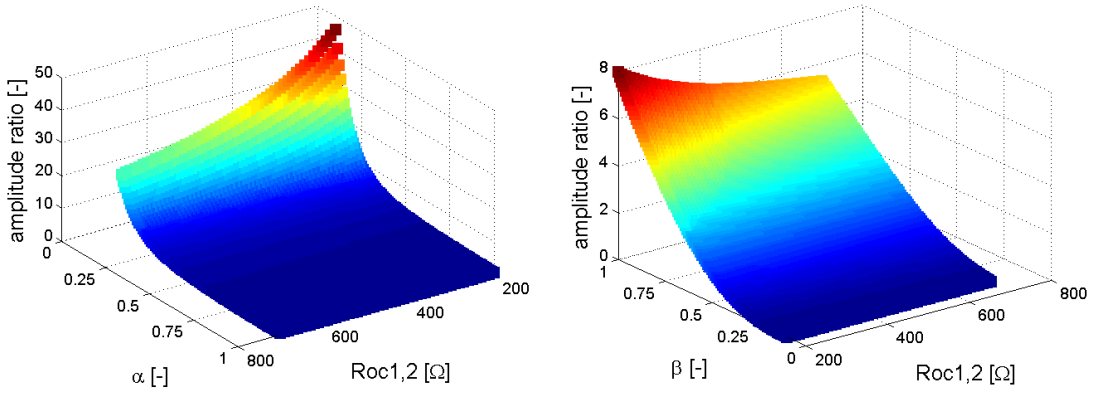

a) b)

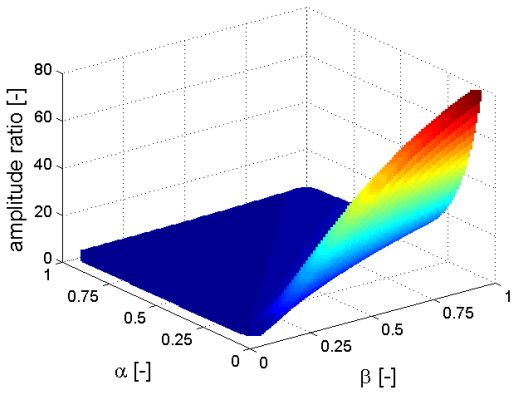

c)

Fig. 17. The 3D analysis of multi-parameter impact (order and parameter for tuning) on amplitude ratio (valid for $C_{\alpha,\beta}$ = 56 µF): a) amplitude ratio vs α and $R_{OC1,2}$, b) amplitude ratio vs β and $R_{OC1,2}$, c) amplitude ratio vs α and β.

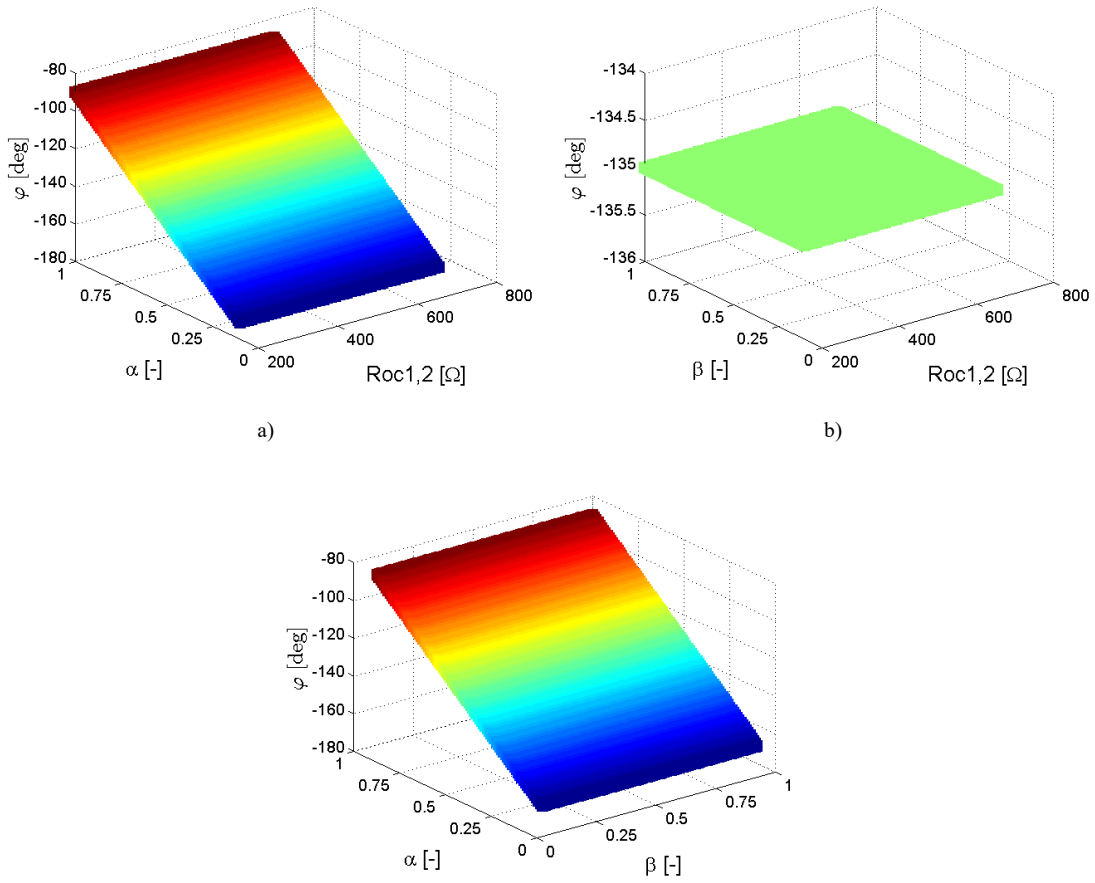

a) b) c)

Fig. 18. The 3D analysis of multi-parameter impact (order and parameter for tuning) on phase shift (valid for $C_{\alpha,\beta}$ = 56 μF): a) phase shift vs α and $R_{OC1,2}$, b) phase shift vs β and $R_{OC1,2}$, c) phase shift vs α and β.

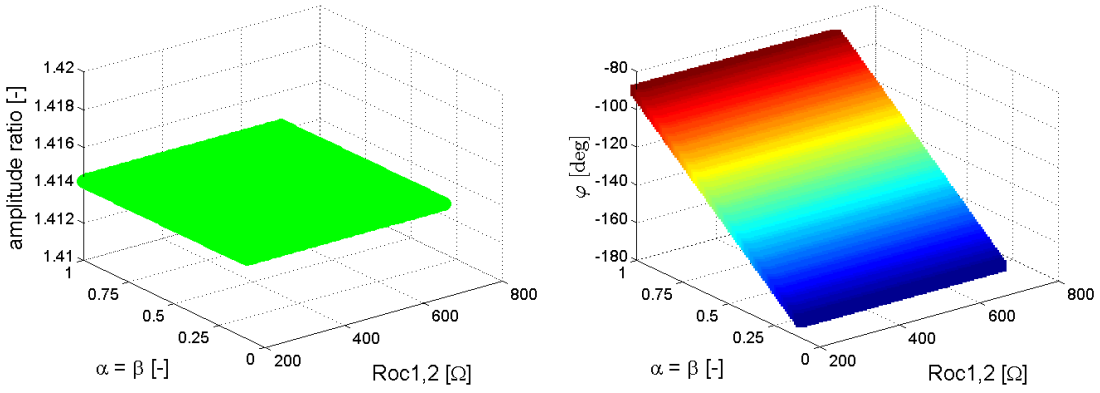

a) b)

Fig. 19. The 3D analysis of multi-parameter impact (order and parameter for tuning): a) amplitude ratio vs α = β and $R_{OC1,2}$, b) phase shift vs α = β and $R_{OC1,2}$.

7. Symbolical sensitivity analysis

The ideal equations (7) and (8) were subjects to sensitivity analysis on variation of parameters included in them. Note that sensitivities to parameters that are not shown below are irrelevant (equal to 0). The

following equations show the results of the analysis of the relative sensitivity of the oscillation frequency (7) on changes of these circuit parameters (R_{OC1}, R_{OC2}, C_a, C_b):

$$S_{rel\_R_{OC1}}^{\omega_0} = \frac{\partial \omega_0}{\partial R_{OC1}} \cdot \frac{R_{OC1}}{\omega_0} = S_{rel\_R_{OC2}}^{\omega_0} = S_{rel\_C_\alpha}^{\omega_0} = S_{rel\_C_\beta}^{\omega_0} = -\left[\alpha + \left(\frac{2\sin\left(\alpha\frac{\pi}{2}\right)}{C_\alpha C_\beta R_{OC1} R_{OC2} \sin\left(\beta\frac{\pi}{2}\right)} \right)^{\frac{1}{\alpha+\beta}} \right]^{-1}. \quad (13)$$

Unfortunately, the analysis of the sensitivity to orders (α, β) variation is not providing applicable results (the expression is very complex and not giving any clear information). The relative sensitivities of the condition (8) on circuit parameters (ω_0, C_β, α, β) are given below:

$$S_{rel\_\omega_0}^{A} = \frac{\partial A(\omega_0)}{\partial \omega_0} \cdot \frac{\omega_0}{A(\omega_0)} = \frac{\beta C_\beta R_n \omega_0^\beta \sin\left((\alpha+\beta)\frac{\pi}{2}\right)}{\sin\left(\alpha\frac{\pi}{2}\right) + C_\beta R_n \omega_0^\beta \sin\left((\alpha+\beta)\frac{\pi}{2}\right)}, \quad (14)$$

$$S_{rel\_C_\beta}^{A} = \frac{\partial A(C_\beta)}{\partial C_\beta} \cdot \frac{C_\beta}{A(C_\beta)} = S_{rel\_R_n}^{A} = \frac{C_\beta R_n \omega_0^\beta \sin\left((\alpha+\beta)\frac{\pi}{2}\right)}{\sin\left(\alpha\frac{\pi}{2}\right) + C_\beta R_n \omega_0^\beta \sin\left((\alpha+\beta)\frac{\pi}{2}\right)}, \quad (15)$$

$$S_{rel\_\alpha}^{A} = \frac{\partial A(\alpha)}{\partial \alpha} \cdot \frac{\alpha}{A(\alpha)} = \frac{\alpha\pi\omega_0^\beta C_\beta R_n \sin\left(\beta\frac{\pi}{2}\right)}{\cos(\alpha\pi) - C_\beta R_n \omega_0^\beta \cos\left(\beta\frac{\pi}{2}\right) + C_\beta R_n \omega_0^\beta \cos\left((2\alpha+\beta)\frac{\pi}{2}\right) - 1}, \quad (16)$$

$$S_{rel\_\beta}^{A} = \frac{\partial A(\beta)}{\partial \beta} \cdot \frac{\beta}{A(\beta)} = \frac{\omega_0^\beta C_\beta R_n \left[\sin\left((\alpha+\beta)\frac{\pi}{2}\right)\log(\omega_0) + \pi\cos\left((\alpha+\beta)\frac{\pi}{2}\right) \right]}{2\left[\sin\left(\alpha\frac{\pi}{2}\right) + \omega_0^\beta C_\beta R_n \sin\left((\alpha+\beta)\frac{\pi}{2}\right) \right]}. \quad (17)$$

Note that the substitution of the symbolical frequency ω_0 (7) into above expressions returns extensive results not providing an easy survey. Substitution of numerical values of parameters (in accordance with exemplary design shown in Section 5) into (13) results in numerical relative sensitivity values: –1 ($R_{OC1,2}$, C_a, C_b), and –3.9 and –5.4 for the orders α and β respectively (not based on (13)). The same substitution to equations (14) – (17) are as follows: 0.45, 0.9, –0.7, 4.2. These results are valid for α = 0.5, $C_\alpha = 56$ μF/sec$^{1/2}$, $R_{OC1,2} \cong 241\ \Omega$, $V_{SET\_FO} \cong 5$ V, $R_n = 1$ kΩ, $\omega_0 = 2\pi \cdot 1750$ rad/s. Note that variation of orders and further parameters included in the functions have an effect on the overall sensitivity because the equations (13)-(17) are multi-parameter functions.

8. Conclusion

In this paper, we analyzed two cases (α = β and α ≠ β) of the implementation of the fractional-order elements in the design of an electronically tunable oscillator (with DC voltage control).

The first case assumes both CPEs to be identical (equivalent capacities and orders). Three particular examples of the values were studied: 1/4, 1/2 and 3/4. The experimental results confirmed the expected behavior: the order significantly helps with the tunability extension (1 kHz →

41 kHz tested for $\alpha = 1/4$); the phase shifts and the ratios between generated amplitudes remain almost constant. Errors of all the obtained values are in correspondence with the influences expected from the accuracy of the CPE approximants (the error below ±5 % in most of the tuning range). The frequency tuning of the scenarios using $\alpha = 3/4$ and 1/2 targets hundreds of Hz and units of kHz.

The second studied case targets the setting with different orders of both CPEs in the design. Such arrangement allows operation in the frequency range up to several kHz. The phase shift between the produced signals is given by C_α and the obtained values of the error compared to the first case are lower (the phase error less by ± 3%). The THD values were in low units of percent in all tests.

The mutual dependence of the frequency and the condition of oscillation (bidirectional, i.e. CO on FO and also FO on CO), typical in the case of fractional-order oscillators, creates an important practical drawback. However, the dependence of the condition on the parameters suitable for the frequency tuning, in this particular way, can be driven by the system for automatic amplitude stabilization and condition control as was shown in this work. Thus, the drawback of the dependence of CO on FO in specific solutions can be effectively suppressed. The using of fractional-order elements can be viewed as a way for a tunability range extension [11], [12], [14], [39]. However, as we can see from many previous works, searching for a practically useful topology is a quite different task.

Note that this work is not prepared for a specific application. Possible applications are supposed in generators of waveforms with specified phase shifts and simultaneously tunable electronically by the driving voltage without any effect of the implementation of the fractional-order elements. This work was more targeted on a study and a proof of what happens (with the amplitude ratio and phase shift) when the orders are varying. Attention is not paid to this topic in many recent works. Moreover, many low-frequency biomedical or audio systems require generation of waveforms having specific phase shifts and immediate electronic tunability without a change of the amplitude and phase shift when tuned. This work documents (the main aim) that some specific types of circuits (unfortunately not all presented in recent literature) can be used in practice with similar features as standard integer-order oscillators and in studies of the behavior caused by variation of many parameters.

Acknowledgement

This article is based upon work from COST Action CA15225, a network supported by COST (European Cooperation in Science and Technology). Research described in this paper was financed by the Ministry of Education, Youth and Sports under grant LTC18022 of Inter-Cost program.

References

[1] A. S. Elwakil, "Fractional-order circuits and systems: An emerging interdisciplinary research area," *IEEE Circ. and Sys. Mag.*, vol. 10, no. 4, pp. 40–50, 2010.

[2] A.G. Radwan, A.S. Elwakil, A.M. Soliman, "Fractional-order sinusoidal oscillators: design procedure and practical examples," *IEEE Trans. on Circuits and Systems I: Regular Papers*, vol. 55, vol. 7, pp. 2051–2063, 2008.

[3] L. A. Said, A. G. Radwan, A. H. Madian, A. M. Soliman, "Fractional order oscillators based on operational transresistance amplifiers," *AEU - International Journal of Electronics and Communications*, vol. 69, no. 7, pp. 988–1003, 2015.

[4] M. Fouda, A. Soltan, A. G. Radwan, A. M. Soliman, "Fractional-order multi-phase oscillators design and analysis suitable for higher-order PSK applications," *Analog Integrated Circuits and Signal Processing*, vol. 87, no. 2, pp. 301–312, 2016.

[5] L. A. Said, A. G. Radwan, A. H. Madian, A. M. Soliman, "Three Fractional-Order-Capacitors-Based Oscillators with Controllable Phase and Frequency," *Journal of Circuits, Systems and Computers*, vol. 26, no. 10, pp. 1750160–1750178, 2017. DOI: 10.1142/S0218126617501602

[6] L.A. Said, A.G. Radwan, A.H. Madian, A.M. Soliman, "Two-port two impedances fractional order oscillators," *Microelectronics Journal*, vol. 55, no. 9, pp. 40–52, 2016.

[7] A. Kartci et al., "Fractional-order oscillator design using unity-gain voltage buffers and OTAs," in *Proc. of 2017 IEEE 60th International Midwest Symposium on Circuits and Systems (MWSCAS)*, Boston, MA, USA, 2017, pp. 555–558.

[8] A. Kartci, N. Herencsar, J. Koton and C. Psychalinos, "Compact MOS-RC voltage-mode fractional-order oscillator design," in *Proc. of European Conference on Circuit Theory and Design (ECCTD)*, Catania, Italy, 2017, pp. 1–4.

[9] A. Kartci, L. Brancik, "CFOA-Based Fractional-Order Oscillator Design and Analysis with NILT Method," in *Proc. of the 27th International Conference Radioelektronika 2017*, Brno, Czech Republic, 2017. pp. 219–222.

[10] A. Kartci, N. Herencsar, L Brancik, K. N. Salama, "CMOS-RC Colpitts Oscillator Design Using Floating Fractional-Order Inductance Simulator," in *Proc. of the 2018 61st IEEE International Midwest Symposium on Circuits and Systems (MWSCAS)*. Windsor, Canada, 2018, pp. 905–908.

[11] A. Kartci, A. Agambayev, A. H. Hassan, H. Bagci, K. N. Salama, "Experimental Verification of a Fractional-Order Wien Oscillator Built Using Solid-State Capacitors," in *Proc. of the 2018 61st IEEE International Midwest Symposium on Circuits and Systems (MWSCAS).* Windsor, Canada, 2018, pp. 544–545.

[12] A. Agambayev, A. Kartci, A. H. Hassan, N. Herencsar, H. Bagci, K. N. Salama, "Fractional-Order Hartley Oscillator," in *Proc. of the 2018 14th Conference on PhD Research in Microelectronics and Electronics (PRIME)*. Prague, Czech Republic, 2018, pp. 45–48.

[13] S. K. Mishra, M. Gupta, D. K. Upadhyay, "Design and implementation of DDCC-based fractional-order oscillator," *Int. J. of Electr. Let.*, vol. 106, no. 4, pp. 581–598, 2019.

[14] A. Kartci, N. Herencsar, J. Dvorak and K. Vrba, "VDIBA-Based Fractional-Order Oscillator Design," In *Proc. of the 2019 42nd International Conference on Telecommunications and Signal Processing (TSP)*, Budapest, Hungary, 2019, pp. 744-747.

[15] S. K. Mishra, M. Gupta,D. K. Upadhyay, "Compact design of four-phase fractional-order oscillator with independent phase and frequency control," *Indian J. of Physics*, vol. 93, pp. 891–901, 2019.

[16] L. A. Said, O. Elwy, A. H. Madian, A. G. Radwan, A. M. Soliman, "Stability analysis of fractional-order Colpitts oscillators," *Analog Integrated Circuits and Signal Processing*, vo. 101, pp. 267–279, 2019.

[17] J. Dvorak, D. Kubanek, J. Koton, J. Jerabek and D. Smekal, "Adjustable Multiphase Sinusoidal Oscillator with Fractional–Order Elements,"in *Proc. of 2019 11th International Congress on Ultra Modern Telecommunications and Control Systems and Workshops (ICUMT)*, Dublin, Ireland, 2019, pp. 1–6.

[18] O. Elwy, L. A. Said, A. H. Madian, A. Radwan, "All Possible Topologies of the Fractional-Order Wien Oscillator Family Using Different Approximation Techniques," *Circuits Systems and Signal Processing*, vol. 38, pp. 3931–3951, 2019.

[19] G. M. Ahmed, L. A. Said, A. H. Madian and A. G. Radwan, "Fractional-Order Oscillators Based on Double Op-Amp," in *Proc. of 2019 Fourth International Conference on Advances in Computational Tools for Engineering Applications (ACTEA)*, Beirut, Lebanon, 2019, pp. 1–4.

[20] G. Tsirimokou, C. Psychalinos, A. Elwakil and B. Maundy, "Fractional-Order Multiphase Sinusoidal Oscillator Design Using Current-Mirrors," in *Proc. of 2018 41st International Conference on Telecommunications and Signal Processing (TSP)*, Athens, 2018, pp. 1-4, doi: 10.1109/TSP.2018.8441399.

[21] A. Pradhan, K. S. Subhadhra, N. Atique, R. K. Sharma and S. S. Gupta, "MMCC-based current-mode fractional-order voltage-controlled oscillators," in *Proc. of 2018 2nd International Conference on Inventive Systems and Control (ICISC)*, Coimbatore, 2018, pp. 763-768, doi: 10.1109/ICISC.2018.8398901

[22] Subhadhra, K.S., Sharma, R.K. & Gupta, S.S. Realisation of some current-mode fractional-order VCOs/SRCOs using multiplication mode current conveyors. *Analog Integr Circ Sig Process* **103,** 31–55 (2020). https://doi.org/10.1007/s10470-020-01590-4

[23] R. Sotner, J. Jerabek, O. Domansky, N. Herencsar, A. Kartci and J. Dvorak, "Practical Design of Fractional-Order Oscillator Employing Simple Resonator and Negative Resistor," in *Proc. of 2018 10th Int. Congress on Ultra Modern Telecommunications and Control Systems and Workshops (ICUMT)*, Moscow, Russia, 2018, pp. 1–4.

[24] A. Adhikary, S. Sen, K. Biswas, "Practical Realization of Tunable Fractional Order Parallel Resonator and Fractional Order Filters," *IEEE Trans. on Circuits and Systems I: Regular Papers*, vol. 63, no. 8, pp. 1142–1151, 2016.

[25] A. Adhikary, S. Choudhary, S. Sen, "Optimal Design for Realizing a Grounded Fractional Order Inductor Using GIC," *IEEE Trans. on Circuits and Systems I: Regular Papers*, vol. 65, no. 8, pp. 2411–2421, 2018.

[26] G. Tsirimokou, C. Psychalinos, A. S. Elwakil and K. N. Salama, "Electronically Tunable Fully Integrated Fractional-Order Resonator," in *IEEE Transactions on Circuits and Systems II: Express Briefs*, vol. 65, no. 2, pp. 166-170, Feb. 2018, doi: 10.1109/TCSII.2017.2684710

[27] P. Huang, M. Tsai, G. D. Vendelin, H. Wang, C. Chen and C. Chang, "A Low-Power 114-GHz Push–Push CMOS VCO Using LC Source Degeneration," *IEEE J. of Solid-State Circ.*, vol. 42, no. 6, pp. 1230-1239, June 2007, doi: 10.1109/JSSC.2007.897136.

[28] D. Biolek, R. Senani, V. Biolkova, Z. Kolka, "Active elements for analog signal processing: Classification, Review and New Proposals," *Radioengineering*, vol. 17, no. 4, pp. 15–32, 2008.

[29] R. Senani, D. R. Bhaskar, and A. K. Singh, Current Conveyors: Variants, Applications and Hardware Implementations. Switzerland: Springer International Publishing, 2015.

[30] J. Valsa, P. Dvorak, M. Friedl, "Network Model of CPE," *Radioengineering*, vol. 20, no. 3, pp. 619–626, 2011.

[31] J. Valsa, J. Vlach, "RC Models of a Constant Phase Element", *Int. J. of Circ. Theo.and Appl.*, vol. 41, no. 1, pp. 59–67, 2013.

[32] R. Sotner, J. Jerabek, L. Langhammer, J. Dvorak, "Design and Analysis of CCII-Based Oscillator with Amplitude Stabilization Employing Optocouplers for Linear Voltage Control of the Output Frequency," *Electronics* (MDPI), vol. 7, no. 9, pp. 1-20, 2018.

[33] O. Domansky, R. Sotner, L. Langhammer, J. Jerabek, C. Psychalinos, G. Tsirimokou, "Practical Design of RC Approximants of Constant Phase Elements and Their Implementation in Fractional-Order PID Regulators Using CMOS Voltage Differencing Current Conveyors," *Circuits, Systems, and Signal Processing*, vol. 38, no. 4, pp. 1520–1546, 2019.

[34] Texas Instruments. VCA810 High Gain Adjust Range, Wideband and Variable gain Amplifier, Accessed: Feb. 25, 2020. [Online]. Available: http://www.ti.com/lit/ds/symlink/vca810.pdf

[35] Analog Devices. 60 Mhz, 2000 V/us Monolithic Op Amp with Quad Low Noise AD844, Accessed: Feb. 25, 2020. [Online]. Available: https://www.analog.com/media/en/technical-documentation/data-sheets/AD844.pdf

[36] Analog Devices. Low Cost 270 MHz Differential Receiver Amplifiers AD8129/8130, Accessed: Feb. 25, 2020. [Online]. Available: https://www.analog.com/media/en/technical-documentation/data-sheets/AD8129_8130.pdf

[37] Texas Instruments. TL07xx Low-Noise JFET-Input General Purpose Operational Amplifiers, Accessed: Feb. 25, 2020. [Online]. Available: https://www.ti.com/lit/ds/symlink/tl072.pdf

[38] Luna Optoelectronics. NSL-32SR3 Optocoupler, Acessed: Feb. 25, 2020. [Online]. Available: https://lunainc.com/wp-content/uploads/2016/06/NSL-32SR3.pdf

[39] R. Sotner, J. Jerabek, N. Herencsar and J. Petrzela, "Methods for Extended Tunability in Quadrature Oscillators Based on Enhanced Electronic Control of Time Constants," *IEEE Trans.on Inst. and Meas.*, vol. 67, no. 6, pp. 1495–1505, 2018.